

Muon Spin Rotation and the Vortex Lattice in Superconductors

Ernst Helmut Brandt^{a,*}

^aMax Planck Institute for Metals Research, D-70506 Stuttgart, Germany

Abstract

The magnetic field probability $P(B)$ is calculated from Ginzburg-Landau theory for various lattices of vortex lines in type-II superconductors: Ideal triangular lattices, lattices with various shear strains and with a super lattice of vacancies, and lattices of short vortices in films whose magnetic field “mushrooms” near the surface.

Key words: Muon Spin Rotation, superconductivity, vortex lattice

1. Introduction

Type-II superconductors like Niobium and many alloys allow magnetic flux to penetrate in form of magnetic flux lines, i.e., vortices of the supercurrent, each vortex carrying one quantum of magnetic flux. This effect was predicted in 1957 by Alexei Abrikosov [1], who got for this the Nobel Prize in Physics 2003. Abrikosov flux lines arrange to a more or less perfect triangular vortex lattice that exhibits interesting structural defects that may be calculated from Ginzburg-Landau (GL) theory [2] or by treating the vortex lattice as a continuum with non-local elasticity [3]. The vortex lattice may even melt into a “vortex liquid” [4]. Pinning of vortices by material inhomogeneities [5] together with thermal fluctuations of the vortices can cause a rich phase diagram in the magnetic field–temperature plane [6], with a melting line and an order–disorder line [7,8] at which the weak elastic disorder (“Bragg glass”) suddenly changes to a plastically deformed or even amorphous vortex arrangement. The vortex lattice can be observed by decoration, magneto-optics, Hall probes, neutron scattering, magnetic force microscopy, and by muon spin rotation (μ SR). μ SR experiments can

give valuable information about the vortex lattice, see the recent review [9].

When pinning and thermal fluctuations may be disregarded (e.g., in clean Niobium with very weak pinning) the vortex lattice exists when the applied magnetic field B_a lies between the lower critical field B_{c1} and the upper critical field B_{c2} . In this interval the internal average induction \bar{B} is smaller than B_a , i.e., the magnetization $M = \bar{B} - B_a$ is negative (diamagnetic behavior), ranging from $-B_{c1}$ to 0 while \bar{B} ranges from 0 to B_{c2} . For $B_a < B_{c1}$ the superconductor expels the magnetic field ($\bar{B} = 0$, ideal Meissner state) and for $B_a > B_{c2}$ the superconductor is in the normal conducting state ($\bar{B} = B_a$). This applies to long superconductor cylinders or slabs in parallel B_a . For other geometries and for inhomogeneous materials, demagnetization effects modify this picture and the magnetization curve in general has to be computed numerically, e.g., for thick or thin strips, disks, and platelets in perpendicular B_a [10]. However, in the particular case when a homogeneous specimen with the shape of an ellipsoid is put into a uniform applied field \mathbf{B}_a , then the demagnetizing field (caused by the magnetization) inside the ellipsoid is also uniform and superimposes to \mathbf{B}_a , thus generating an effective applied field

$$\mathbf{B}_i = \mathbf{B}_a - N\mathbf{M}(\mathbf{B}_i; N = 0). \quad (1)$$

* email: ehb@mf.mpg.de

Solving Eq. (1) for the effective internal field \mathbf{B}_i , one obtains $\mathbf{M} = \mathbf{M}(\mathbf{B}_a; N) = \mathbf{M}(\mathbf{B}_i; N = 0)$. Here N is the demagnetization factor, and the ideal magnetization curve $[M(B_a; 0)$ for $N = 0$, e.g., from GL theory] should be inserted. In general, N is a tensor, but when B_a is along one of the three principal axes of the ellipsoid, then N and all fields in (1) are scalars. For long cylinders or slabs in parallel B_a one has $N = 0$, for spheres $N = 1/3$, for long cylinders in perpendicular field $N = 1/2$, and for thin plates and films one has $1 - N \ll 1$. The sum of the N along the three axes is always $N_1 + N_2 + N_3 = 1$. For the Meissner state one finds $\bar{B} = 0$, $M(B_a; 0) = -B_a$, $B_i = B_a/(1 - N)$, and $M(B_a; N) = -B_a/(1 - N)$, which means the vortex penetration starts at the effective penetration field $B'_{c1} = (1 - N)B_{c1}$ where $B_i = B_{c1}$. In the interval $B'_{c1} < B_a < B_{c2}$ such a pin-free ellipsoid contains a perfect vortex lattice.

In this paper the probability $P(B)$ that at a random point inside the superconductor a muon sees an induction value B , is considered for ideal triangular vortex lattices and for various possible perturbations of it, namely, various types of shear deformation [11], a super lattice of vortex vacancies, the surfaces of a film in a perpendicular field, and random displacements. This probability (or field density) is defined as the spatial average

$$P(B') = \langle \delta(B' - B(\mathbf{r})) \rangle_{\mathbf{r}}. \quad (2)$$

In it B' is the independent variable, $B(\mathbf{r})$ the spatially varying magnetic field, and $\delta(x)$ is the 1D delta function, which for computation may be replaced by a narrow Gaussian whose width may depend on B' . One easily shows that

$$\int_{-\infty}^{\infty} P(B) dB = 1, \quad \int_{-\infty}^{\infty} P(B) B dB = \bar{B}, \quad (3)$$

2. 2D ideal triangular vortex lattice

The local magnetic field $B(x, y)$ of the vortex lattice may be calculated for all values of the reduced average induction $b = \bar{B}/B_{c2}$ and Ginzburg-Landau parameter κ by an elegant iteration method that minimizes the GL free energy F with respect to the Fourier coefficients of the periodic solutions $B(x, y)$ and order parameter $\omega(x, y) = f^2 = |\psi|^2$ where $\psi(x, y) = f \exp(i\varphi)$ is the complex GL function [12,13]. In the usual reduced units (length λ , induction $\sqrt{2}B_c$, energy density B_c^2/μ_0 , where λ is the magnetic penetration depth and $B_c =$

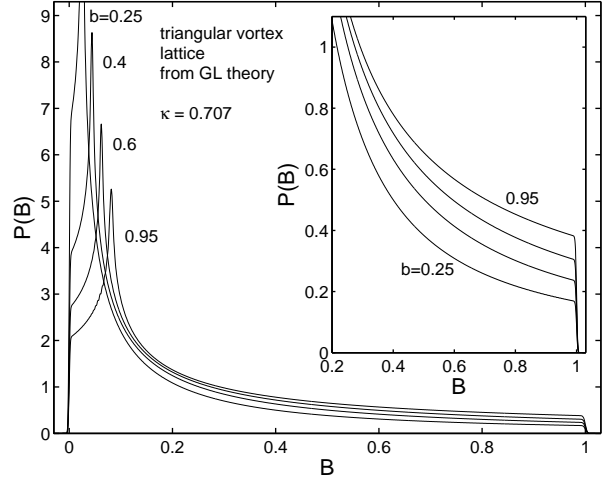


Fig. 1. The field density $P(B)$ of the ideal triangular vortex lattice obtained from GL theory for $\kappa = 1/\sqrt{2} = 0.707$ and $b = 0.25$ to 0.95 . Here and in the figures below the variable B is normalized such that $B = 0$ means B_{\min} and $B = 1$ means B_{\max} , and the inset enlarges the region near B_{\max} .

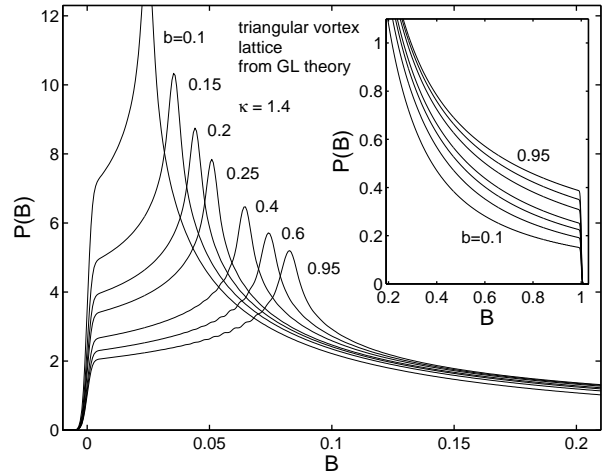


Fig. 2. The $P(B)$ as in Fig. 1 but for $\kappa = 1.4$.

$B_{c2}/\sqrt{2}\kappa$ is the thermodynamic critical field with $B_{c2} = \Phi_0/(2\pi\xi^2)$, $\xi = \lambda/\kappa$ the coherence length and $\Phi_0 = h/2e = 2.07 \cdot 10^{-15}$ Tm² the quantum of magnetic flux) the spatially averaged free energy density F of the GL theory referred to the Meissner state ($\psi = 1$, $\mathbf{B} = 0$) in the superconductor reads

$$F = \left\langle \frac{(1 - |\psi|^2)^2}{2} + \left| \left(\frac{\nabla}{i\kappa} - \mathbf{A} \right) \psi \right|^2 + \mathbf{B}^2 \right\rangle. \quad (4)$$

Here $\mathbf{B}(\mathbf{r}) = \nabla \times \mathbf{A}$, $\mathbf{A}(\mathbf{r})$ is the vector potential, and $\langle \dots \rangle = (1/V) \int_V d^3r \dots$ means spatial averaging over the superconductor with volume V . Intro-

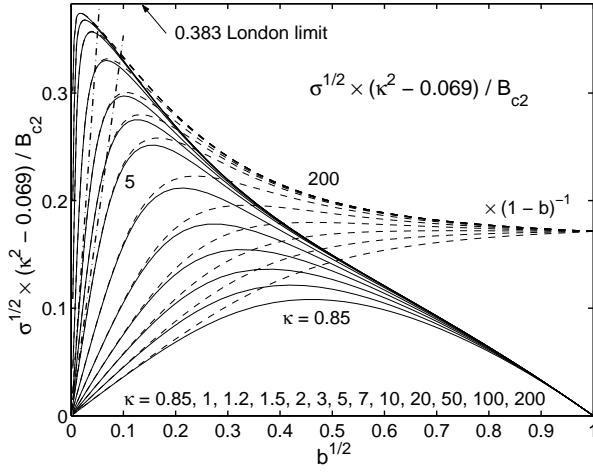


Fig. 3. The magnetic field variance $\sigma = \langle [B(x, y) - \bar{B}]^2 \rangle$ of the triangular FLL for $\kappa = 0.85$ to 200 plotted in units of B_{c2} as $\sqrt{\sigma} \cdot (\kappa^2 - 0.069) / B_{c2}$ (solid lines) such that the curves for all κ collapse near $b = 1$. The dashed lines show the same functions divided by $(1 - b)$ such that they tend to a finite constant 0.172 at $b = 1$. All curves are plotted versus $\sqrt{b} = \sqrt{\bar{B} / B_{c2}}$ to stretch them at small b values and show that they go to zero linearly. The upper frame 0.383 is the usual London approximation. The limit for very small b is shown as two dash-dotted straight lines for $\kappa = 5$ and $\kappa = 10$. The upper frame 0.383 shows the usual London approximation.

ducing the super velocity $\mathbf{Q}(\mathbf{r}) = \mathbf{A} - \nabla\varphi/\kappa$ and the magnitude $f(\mathbf{r}) = |\psi|$ one may write F as a functional of these real and gauge-invariant functions,

$$F = \left\langle \frac{(1 - f^2)^2}{2} + \frac{(\nabla f)^2}{\kappa^2} + f^2 Q^2 + (\nabla \times \mathbf{Q})^2 \right\rangle. \quad (5)$$

In the presence of vortices $\mathbf{Q}(\mathbf{r})$ has to be chosen such that $\nabla \times \mathbf{Q}$ has the appropriate singularities along the vortex cores, where f vanishes. By minimizing this F with respect to ψ , \mathbf{A} or f , \mathbf{Q} , one obtains the two GL equations together with the appropriate boundary conditions. For periodic lattices with one flux quantum per vortex, in the sense of a Ritz variational method one uses Fourier series for the periodic trial functions with a finite number of Fourier coefficients $a_{\mathbf{K}}$ and $b_{\mathbf{K}}$,

$$\omega(\mathbf{r}) = \sum_{\mathbf{K}} a_{\mathbf{K}} (1 - \cos \mathbf{K}\mathbf{r}), \quad (6)$$

$$B(\mathbf{r}) = \bar{B} + \sum_{\mathbf{K} \neq 0} b_{\mathbf{K}} \cos \mathbf{K}\mathbf{r}, \quad (7)$$

$$\mathbf{Q}(\mathbf{r}) = \mathbf{Q}_A(\mathbf{r}) + \sum_{\mathbf{K} \neq 0} b_{\mathbf{K}} \frac{\hat{\mathbf{z}} \times \mathbf{K}}{K^2} \sin \mathbf{K}\mathbf{r}, \quad (8)$$

where $\mathbf{K} = \mathbf{K}_{mn} = (K_x, K_y)$ are the reciprocal lattice vectors of the vortex lattice with positions \mathbf{R}_{mn} ,

$$\mathbf{R}_{mn} = (mx_1 + nx_2; ny_2), \quad (9)$$

$$\mathbf{K}_{mn} = (2\pi/x_1 y_2)(my_2; -mx_2 + nx_1), \quad (10)$$

($m, n = 0, \pm 1, \pm 2, \dots$; triangular lattice: $x_1 = a$, $x_2 = x_1/2$, $y_2 = x_1\sqrt{3}/2$; square lattice: $x_1 = y_2 = a$, $x_2 = 0$). In (8) $\mathbf{Q}_A(x, y)$ is the supervelocity of the Abrikosov B_{c2} solution, which satisfies

$$\nabla \times \mathbf{Q}_A = \left[\bar{B} - \Phi_0 \sum_{\mathbf{R}} \delta_2(\mathbf{r} - \mathbf{R}) \right] \hat{\mathbf{z}}, \quad (11)$$

where $\delta_2(\mathbf{r}) = \delta(x)\delta(y)$ is the 2D delta function. This shows that \mathbf{Q}_A is the velocity field of a lattice of ideal vortex lines but with zero average rotation. Close to each vortex center one has $\mathbf{Q}_A(\mathbf{r}) \approx \mathbf{r}' \times \hat{\mathbf{z}} / (2\kappa r'^2)$ and $\omega(\mathbf{r}) \propto r'^2$ with $\mathbf{r}' = \mathbf{r} - \mathbf{R}$. We take \mathbf{Q}_A from the exact relation

$$\mathbf{Q}_A(\mathbf{r}) = \frac{\nabla \omega_A \times \hat{\mathbf{z}}}{2\kappa \omega_A}, \quad (12)$$

where $\omega_A(x, y)$ is the Abrikosov B_{c2} solution given by a rapidly converging series (6) with coefficients $a_{\mathbf{K}}^A = -(-)^{mn+m+n} \exp(-K_{mn}^2 x_1 y_2 / 8\pi)$. The solutions $\omega(\mathbf{r})$ and $B(\mathbf{r})$ are then computed by iterating equations for the coefficients $a_{\mathbf{K}}$ and $b_{\mathbf{K}}$ that are derived from the GL equations $\delta F / \delta \omega = 0$ and $\delta F / \delta \mathbf{Q} = 0$. This method and the obtained GL solutions are presented in detail in [12,13].

The field density $P(B)$ of the ideal triangular vortex lattice is shown for several $b = \bar{B} / B_{c2}$ values in Fig. 1 ($\kappa = 1/\sqrt{2}$) and Fig. 2 ($\kappa = 1.4$). For larger κ the $P(B)$ look similar to Fig. 2. For small b and large κ the $P(B)$ obtained from the London approximation are depicted in [11]. The maximum and the 2 equal minima per unit cell yield two steps in $P(B)$ at $B = B_{\max}$ ($=1$) and $B = B_{\min}$ ($=0$), and the 3 equal saddle points yield a logarithmic infinity at $B = B_{\text{sad}}$ where $P(B) \propto -\ln |B - B_{\text{sad}}|$.

The variance of the magnetic field, $\sigma = \langle [B(x, y) - \bar{B}]^2 \rangle = \sum_{\mathbf{K} \neq 0} b_{\mathbf{K}}^2$, is plotted for the entire ranges of b and κ in Fig. 3. In the low-field range $0.13/\kappa^2 \ll b \ll 1$ one has for the triangular lattice the London limit $\sigma = 0.00371 \Phi_0^2 / \lambda^4$ (upper frame in Fig. 3), at very small $b \ll 0.13/\kappa^2$ one has $\sigma = (b\kappa^2 / 8\pi^2) \Phi_0^2 / \lambda^4$ (dash-dotted straight lines in Fig. 3), and near $b = 1$ one has the Abrikosov limit $\sigma = 7.52 \cdot 10^{-4} (\Phi_0^2 / \lambda^4) [\kappa^2 (1 - b) / (\kappa^2 - 0.069)]^2$, approximately valid even at $b \gtrsim 0.3$, see [13]. Note that the usual London limit for σ applies only in a narrow range of small (but not too small) b and

for $\kappa > 50$. The same is true for the London limit of the magnetization curve, where the often used “logarithmic law valid at $B_{c1} \ll B_a \ll B_{c2}$ ” for $M(B_a) = \bar{B} - B_a$ has a small range of validity [13].

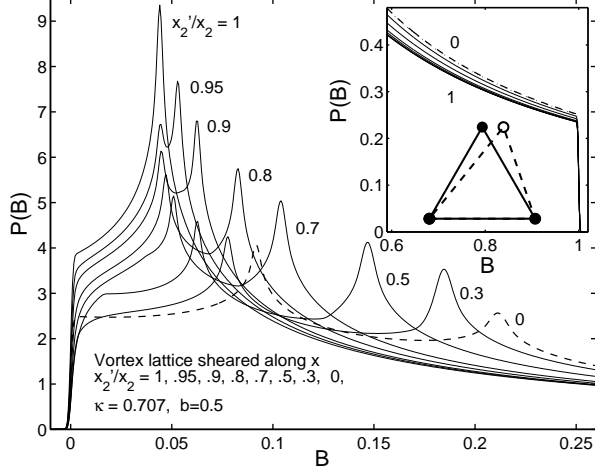


Fig. 4. Vortex lattice sheared along the x axis.

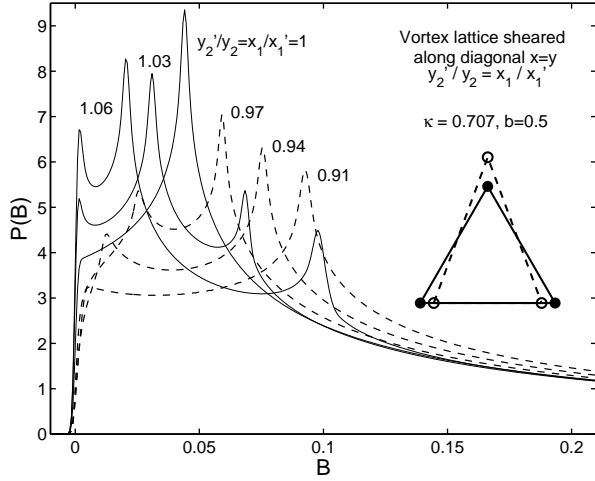


Fig. 5. Vortex lattice sheared along the diagonal $x = y$.

3. Sheared vortex lattices

The above Fourier method applies to any vortex lattice symmetry with vortex positions \mathbf{R}_{mn} (9), also to sheared triangular lattices and to square and rectangular basic cells. In Fig. 4 the field density $P(B)$ is shown for a lattice sheared away from the ideal triangular lattice by decreasing in Eq. (9) the length $x_2 = 0.5$ by a factor $c = x'_2/x_2 = 1$ (triangular), 0.95, 0.9, ..., 0 (rectangular lattice).

With $y_2 = \sqrt{3}/2$ the shear strain in these cases is $\gamma = (1 - c)x_2/y_2 = (1 - c)/\sqrt{3}$. Note that for this shear the saddle point peak splits into 2 peaks, i.e., there are now two different types of saddle points in $B(x, y)$, but still one maximum and 2 equal minima. Figure 5 shows a different orientation of shearing the triangular lattice, namely, now the lengths y_2 and x_1 are changed by a factor $c = y'_2/y_2 = x'_1/x'_1 = 1.06, 1.03, 1, 0.97, 0.94, 0.91$ such that the unit cell area $x_1y_2 = x'_1y'_2$ does not change (no compression). This corresponds to a shear strain of size $\gamma = 2(1 - c)$ oriented along the diagonal $x = y$. One can see that for $c > 1$ the saddle point peak splits into 3 peaks (i.e. all 3 saddle points now occur at different B) while for $c < 1$ there occur 2 different saddle point peaks.

One notes that even very small shear of the vortex lattice causes pronounced change in the field probability $P(B)$. Small shear costs very little energy since the shear modulus c_{66} of the vortex lattice is much smaller than its compressional modulus c_{11} or its tilt modulus c_{44} . One has approximately [3]

$$c_{11}(k) = \frac{\bar{B}^2}{\mu_0} \frac{\partial B_a}{\partial \bar{B}} \frac{1}{(1 + k^2 \lambda'^2)} + c_{66} \quad (13)$$

$$c_{66} \approx \frac{\bar{B} B_{c2}}{8\kappa^2 \mu_0} \frac{(1 - b)^2 (2\kappa^2 - 1) 2\kappa^2}{(2\kappa^2 - 1 + 1/\beta_A)^2} \quad (14)$$

$$c_{44}(k) = \frac{\bar{B}^2}{\mu_0} \frac{1}{1 + k^2 \lambda'^2} + \frac{\bar{B}(B_a - \bar{B})}{\mu_0} \quad (15)$$

with $\lambda' = \lambda/\sqrt{1 - b}$. In c_{66} , $\beta_A = 1.1596$ is the Abrikosov parameter of the triangular lattice (the square lattice is unstable and thus has negative c_{66}), and the factor $(2\kappa^2 - 1)$ means the shear stiffness of the vortex lattice is zero in superconductors with $\kappa = 0.707$ (pure Nb).

An interesting property is the dependence of c_{11} (13) and c_{44} (15) on the magnitude $k = |\mathbf{k}|$ of the wave vector $\mathbf{k} = (k_x, k_y, k_z)$ of spatially periodic strain, which means the elasticity of the vortex lattice is **non-local**. In the limit of uniform stress, $k \rightarrow 0$, these expressions reproduce the known values of the uniform compression and tilt moduli obtained by thermodynamics, $c_{11} - c_{66} = (\bar{B}^2/\mu_0)\partial B_a/\partial \bar{B}$, $c_{44} = \bar{B}B_a/\mu_0$. However, when the wavelength of the periodic compression or tilt decreases, i.e., k increases, these moduli decrease. This means, the vortex lattice is softer for short-wavelengths compression and tilt than it is for long wavelengths. In anisotropic superconductors these moduli at finite wavelengths are even smaller [14] and the vortex lattice is softer and can be distorted and melted more easily in high- T_c superconductors.

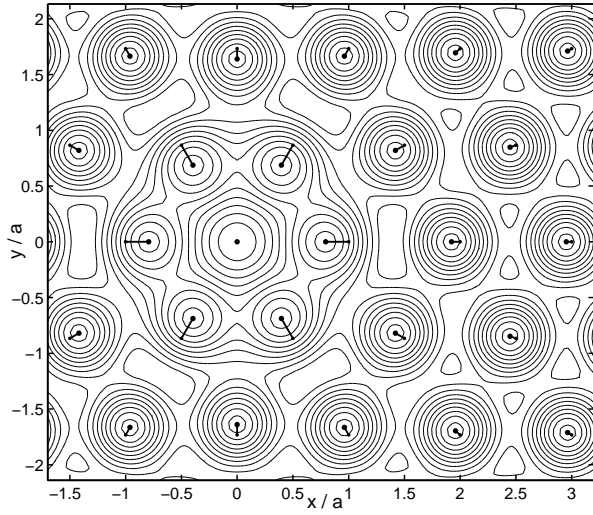


Fig. 6. Contour lines of order parameter $\omega(x, y)$, Eq. (17), identical to the contours of induction $B(x, y)$, Eq. (16), for a vortex lattice with one vacancy. The displacements \mathbf{s}_ν of the relaxing vortices are shown as short bold lines connecting two dots. At all vortex positions $\omega(x, y)$ has a minimum and is zero, but at the origin $x = y = 0$, ω is maximum since a vortex was removed from there.

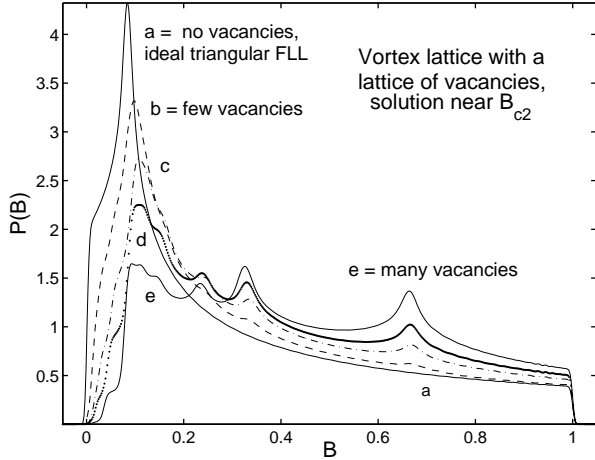


Fig. 7. $P(B)$ Field density $P(B)$ of a vortex lattice with various vacancy concentrations $1/N^2$: a) no vacancy, b) $N = 9$, c) $N = 6$, d) $N = 4$, e) $N = 3$. GL solution near B_{c2} .

4. Vortex lattice containing vacancies

As an example for structural defects I consider a vortex lattice (spacing a) with a super lattice of vacancies with spacing Na , $N = 2, 3, 4, \dots$. This problem was solved in [2] both within London theory (at $b \ll 1$) and GL theory near $b = 1$ where

$$B(\mathbf{r}) = \bar{B} + [\langle \omega \rangle - \omega(\mathbf{r})] B_{c2} / (2\kappa^2) \quad (16)$$

holds, i.e., the shapes of $\omega(x, y)$ and $B(x, y)$ are the same. For this vacancy lattice near $b = 1$ one has

$$\omega(\mathbf{r}) = c_1 \frac{\omega_A(\mathbf{r})}{\omega_A(\mathbf{r}/N)} \prod_{\nu} \frac{\omega_A[(\mathbf{r} - \mathbf{R}_{\nu} - \mathbf{s}_{\nu})/N]}{\omega_A[(\mathbf{r} - \mathbf{R}_{\nu})/N]}, \quad (17)$$

where $\omega_A(x, y)$ is the Abrikosov B_{c2} solution given below Eq. (12), c_1 is a normalization constant, the product is over all vortex positions $\mathbf{R}_{\nu} = \mathbf{R}_{mn}$ within the super cell, and the vortex displacements \mathbf{s}_{ν} are chosen such as to minimize the free energy and the Abrikosov parameter $\beta = \langle \omega^2 \rangle / \langle \omega \rangle^2 > 1$. This relaxation of the vortex positions around the vacancy yields an $\omega(x, y)$ with nearly constant spatial amplitude, i.e., the maximum $\omega(0, 0)$ at the vacancy position has about the same height as all the maxima of ω between the vortices.

Figure 6 shows the contours of ω (and thus of B) for a vortex lattice with one vacancy (limit $N \rightarrow \infty$) at the origin and with central symmetric displacements $\mathbf{s}_{\nu} = -\mathbf{R}_{\nu} [\sqrt{3}a^2 / (4\pi R_{\nu}^2) + 0.068a^4 / R_{\nu}^4]$. The field density $P(B)$ of vortex lattices with various vacancy concentrations $1/N^2$ is shown in Fig. 7. The new peaks indicate that new saddle points and minima of $B(x, y)$ (i.e., maxima of ω) appear near the vacancy, as seen also in Fig. 6.

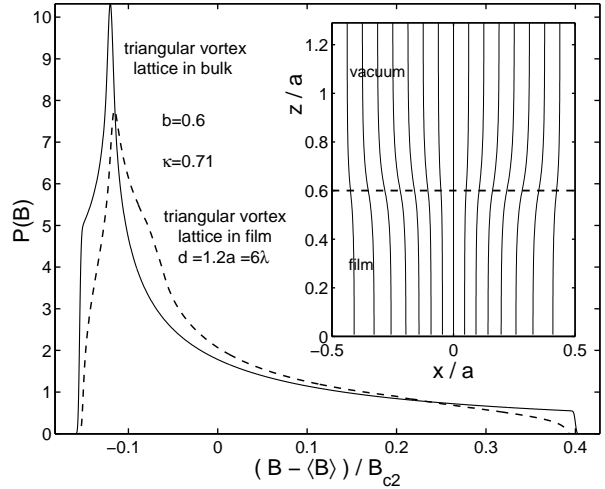


Fig. 8. The field density $P(B)$ of the triangular vortex lattice in a superconducting film of thickness $d = 1.2a = 6\lambda$ in a perpendicular field $B_a = \bar{B}$ for $\kappa = 0.707$, $b = \bar{B}/B_{c2} = 0.6$, from GL theory. Shown are $P(B)$ for bulk (2D, solid line) and for film (3D, dashed line). The inset shows the magnetic field lines in and near the film; the dashed line marks the film surface $z = d/2 = 0.6a$, $a =$ vortex spacing.

5. 3D vortex lattice in films

The Fourier method of Sec. 2 may be generalized to superconducting films of arbitrary thickness d ($|z| \leq d/2$) containing a vortex lattice that is periodic in the (x, y) plane. For this one has to add to F , Eq. (5), the energy F_{stray} of the magnetic stray field outside the film and has to use z dependent trial functions, e.g., (6)-(8) with Fourier coefficients depending on 3D vectors $\mathbf{K} = (K_x, K_y, K_z)$ [15]. When the applied field B_a is along z (perpendicular to the film plane) then the short vortex lines are straight and along z . The inset of Fig. 8 shows how the magnetic field lines of the vortices become less dense when they approach the film surface, they “mushroom” and go over smoothly into the stray field.

Though in the depicted example ($b = 0.6$, $\kappa = 0.707$, $d = 1.2a \approx 6\lambda \approx 4\xi$) this widening of the field lines is only weak, it still has a strong effect on the field density $P(B)$ shown as dashed line, namely, the jumps of B_{min} and B_{max} and the saddle-point peak are smeared and shifted towards \bar{B} , and $P(B)$ is increased (has a hump) between $B = B_{\text{sad}}$ and \bar{B} . These features are expected since for very thin films with $d < \lambda$ the field amplitude is strongly reduced inside the film and $P(B)$ narrows to a line positioned at $B = \bar{B}$. This $P(B)$ should be observable by μSR in specimens composed of many thin layers separated by a distance $\geq a/4$ where the stray-field modulation amplitude $\propto \exp[-2\pi(|z| - d/2)/a]$ has almost vanished.

In such infinitely extended films one has $\bar{B} = B_a$ since all field lines have to pass the film. The magnetization M of the film, therefore, cannot be calculated as a difference of fields, but one has to take the derivative of the total free energy, $M = -\partial(F + F_{\text{stray}}/d)/\partial B$. A more elegant method calculates M by Doria’s virial theorem directly from the GL solution for the film, with no need to take an energy derivative [16].

6. Random perturbations

In real superconductors randomly positioned weak pinning centers, or random pinning forces, may lead to more or less random small displacements of the vortices from their ideal lattice positions. As shown in [11], in bulk superconductors this leads approximately to a convolution of the ideal-lattice $P(B)$ with a Gaussian. Computer sim-

ulations of this problem based on London theory (i.e., pairwise interacting vortex lines and linear superposition of vortex fields) are presented in [11]. Interestingly, while disorder of a 2D vortex lattice **broadens** $P(B)$ and its singularities, disorder in the 3D point-vortex (or pancake-vortex) lattice occurring in layered high- T_c superconductors [6,17] typically will lead to **narrowing** of $P(B)$ [18] since the vortex lines (pancake stacks) become wider. A further effect that contributes to the broadening of $P(B)$ is the (quantum) diffusion of muons after they have stopped, e.g., in ultrapure Nb [19–21].

Improved pinning simulations using GL theory and considering also **thermal fluctuations** of vortices are desirable, as well as microscopic calculations going beyond the GL approach. From BCS-Gor’kov theory it is shown in [11,19] that for pure Nb near B_{c2} the $P(B)$ depends on temperature T , and at $T \ll T_c$ it looks quite different from the GL result valid near the critical temperature T_c since then $B(x, y)$ has sharp conical maxima and minima, and two saddle points with three-fold symmetry yielding an infinity of the form $P(B) \propto |B - B_{\text{sad}}|^{-1/3}$.

References

- [1] A. A. Abrikosov, Zh. Exp. Teor. Fiz. **32**, 1442, 1957 (Sov. Phys.-JETP **5**, 1174, 1957).
- [2] E. H. Brandt, phys. stat. sol. **35**, 1027 (1969); **36**, 371 (1969); **36**, 381 (1969); **36**, 393 (1969).
- [3] E. H. Brandt, J. Low. Temp. Phys. **26**, 709 (1977); **26**, 735 (1977); **28**, 263 (1977); **28**, 291 (1977).
- [4] E. Zeldov et al., Nature **375**, 373 (1995).
- [5] A. M. Campbell and J. E. Evetts, Adv. Phys. **21**, 199 (1972).
- [6] G. Blatter, M.V. Feigel’man, V.B. Geshkenbein, A.I. Larkin, V.M. Vinokur, Rev. Mod. Phys. **66** (1994) 1125.
- [7] K. Shibata, T. Nishizaki, T. Sasaki, N. Kobayashi, Phys. Rev. B **66**, 214518 (2002).
- [8] G. P. Mikitik and E. H. Brandt, Phys. Rev. B **64** 184514 (2001); dito **68**, 054509 (2003)
- [9] I. L. Landau and H. Keller, Phys. C **466**, 131 (2007).
- [10] E. H. Brandt, Phys. Rev. B **64**, 024505 (2001).
- [11] E. H. Brandt, J. Low Temp. Phys. **73**, 355 (1988).
- [12] E. H. Brandt, Phys. Rev. Lett. **78**, 2208 (1997).
- [13] E. H. Brandt, Phys. Rev. B **68**, 054506 (2003).
- [14] E. H. Brandt, Rep. Prog. Phys. **58**, 1465-1594 (2003).
- [15] E. H. Brandt, Phys. Rev. B **71**, 014521 (2005).
- [16] M. M. Doria, E. H. Brandt, and F. M. Peeters, Phys. Rev. B (in print).
- [17] J. R. Clem, Phys. Rev. B **43**, 7837 (1991).
- [18] E. H. Brandt, Phys. Rev. Lett. **66**, 3213 (1991).
- [19] E. H. Brandt and A. Seeger, Adv. Physics **35**, 189 (1986).
- [20] A. Schwarz et al., Hyperfine Interact. **31**, 247 (1987).
- [21] D. Herlach et al., Hyperfine Interact. **63**, 41 (1990).